Environmental Science Nano

PAPER

View Article Online
View Journal | View Issue



Cite this: *Environ. Sci.: Nano*, 2017, 4, 2388

# Structure–activity relationship of surface hydroxyl groups during $NO_2$ adsorption and transformation on $TiO_2$ nanoparticles†

Chang Liu, ‡[ab] Qingxin Ma, ‡[ac] Hong He,‡*[ac] Guangzhi He, ‡[a] Jinzhu Ma,[ac] Yongchun Liu[ac] and Ying Wu[a]

Received 30th September 2017,
Accepted 1st November 2017

DOI: 10.1039/c7en00920h

rsc.li/es-nano

The role of hydroxyl groups (OH) is significant in understanding the surface reactions on oxides. Here we combined spectroscopic experiments and theoretical calculations to reveal the role of OH in the heterogeneous reactions of $NO_2$ on $TiO_2$ nanoparticles with various crystal structures. The interaction between OH and $NO_2$ was determined to be a critical step, giving rise to the formation of surface $HNO_3$. $HNO_3$ was found to be either a stable product on amorphous $TiO_2$, or an important intermediate of nitrate on anatase due to its further reaction with nearby OH. The lack of surface OH on rutile limited its reactivity toward $NO_2$. This study presents clear evidence that the reactivity of $TiO_2$ toward $NO_2$ greatly depends on the surface OH as well as the crystalline form. Considering the ubiquitous presence of $TiO_2$ nanoparticles in catalysts and in natural environments, our results could provide insights helpful to future research in both environmental catalysis and atmospheric chemistry.

**Environmental significance**

With the increasing interest in the removal of $NO_x$ (NO and $NO_2$), $TiO_2$ nanoparticles and $TiO_2$-based catalysts have been reported to be efficient materials for $NO_x$ abatement. Previous mechanistic studies revealed that hydroxyl groups (OH) are ubiquitous on the $TiO_2$ surface and could act as reactive sites. However, the role of OH remains controversial due to the multiplicity and complexity of these OH species. In this study, we observed an excellent example illustrating the structure–activity relationship of OH in the adsorption and reaction of $NO_2$ on $TiO_2$ nanoparticles. It is demonstrated that the crystal phase of $TiO_2$ determines the nature of the surface OH, which then determines the reaction pathway of $NO_2$ on $TiO_2$. Considering the wide usage of $TiO_2$ nanoparticles in environmental chemistry, this work could provide a new approach to design $TiO_2$-based catalysts with superior catalytic performance.

## Introduction

Interfaces in natural and anthropogenic oxide particles are usually covered with hydroxyl groups (OH) formed by the dissociative chemisorption of water. These OH groups act as effective adsorptive or reactive sites for adsorbed substances, and can even dominate the activity of these substances. Therefore, the chemistry of OH groups has been a major concern in environmental catalysis and surface chemistry.

The different types of surface hydroxyls are not fully equivalent structurally or chemically. It has been proposed that the types of OH groups on oxides include terminal, bridging, and triple bridging configurations according to their coordination states.[1] Typically, surface OH groups are considered to be basic and nucleophilic, and these properties are greatly dependent on the coordination structure.[2] Gas probes, such as CO, $CO_2$, $SO_2$, pyridine, and so on, have been used to characterize the properties of surface OH groups, and have shown that the terminal OH group may be more basic than the others.[2] However, the multiplicity and the complexity of hydroxyl groups still present great challenges for research on OH-related reactions. Here, we used the heterogeneous reaction of $NO_2$ on $TiO_2$ as a probe reaction to explore the role of different types of OH groups in surface chemistry.

$NO_2$ plays a key role in atmospheric chemistry. It initiates the photochemical production of $O_3$ in daytime,[3] depletes $O_3$ and produces $NO_3$ radicals at night,[4] leads to the formation of nitric acid and nitrate aerosols,[5] contributes to the sources of OH radicals *via* forming HONO,[6] and causes respiratory

[a] *State Key Joint Laboratory of Environment Simulation and Pollution Control, Research Center for Eco-Environment Sciences, Chinese Academy of Sciences, Beijing 100085, China. E-mail: honghe@rcees.ac.cn; Fax: +86 10 62923563; Tel: +86 10 62849123*
[b] *State Key Laboratory of Severe Weather & Key Laboratory of Atmospheric Chemistry of China Meteorological Administration, Chinese Academy of Meteorological Sciences, Beijing 100081, China*
[c] *Center for Excellence in Urban Atmospheric Environment, Institute of Urban Environment, Chinese Academy of Sciences, Xiamen 361021, China*
† Electronic supplementary information (ESI) available. See DOI: 10.1039/c7en00920h
‡ These authors contributed equally to this work.

diseases in polluted regions.[7] Therefore, the transformation and elimination of $NO_2$ is of significant environmental and health importance.

With the increasing interest in the removal of $NO_x$ (NO and $NO_2$), $TiO_2$, which is a multifunctional material widely used as a heterogeneous catalyst[8] and photo-catalyst[9] as well as in solar cells[10] and gas sensors,[11] has been reported to be an effective material for $NO_x$ removal. $TiO_2$-based catalysts have been widely used in the catalytic reduction of $NO_x$.[12,13] $TiO_2$ is also considered an environmentally friendly material and is added to building walls and roads for the efficient photocatalytic removal of $NO_x$ under ambient conditions.[14] Moreover, $TiO_2$ can alter the cycling of $NO_x$ by providing a medium for heterogeneous and photochemical reactions in the biosphere, since it is an important component of crustal soil and mineral dust.[15,16] Thus, the adsorption and reaction of $NO_2$ on $TiO_2$ surfaces has attracted much attention in both $NO_x$ removal technology and $NO_x$ atmospheric chemistry.

Previous mechanistic studies revealed that both Ti sites[17–19] and surface hydroxyl groups[20–23] could be active sites for the $NO_2$ reaction on $TiO_2$. A well-accepted mechanism of $NO_2$ adsorption on $TiO_2$ *via* Ti sites is as follows. The adsorption of $NO_2$ on Ti sites leads to the formation of nitrite. Nitrite can then react with another surface nitrite (Langmuir–Hinshelwood type) or gas-phase $NO_2$ (Eley–Rideal type), resulting in the formation of surface nitrate and gas-phase NO under dark conditions.[18] On the other hand, the surface hydroxyl groups on $TiO_2$ were also established to be quite active and have a nearly complete reactivity toward $NO_2$.[22] Hydroxyl groups were found to increase the efficacy of the $NO_2$ reaction by reacting with three $NO_2$ molecules *via* disproportionation, leaving two nitrate ions and one molecule of NO.[20–22] Previous infrared spectroscopic studies demonstrated that more than one type of hydroxyl group is consumed during the $NO_2$ reaction on $TiO_2$.[22,23] However, the exact role of each type of OH on the adsorption and reaction of $NO_2$ on $TiO_2$ is still not clear.

The present study aims to recognize the multiplicity of surface hydroxyls on $TiO_2$ and determine the significance of each hydroxyl species in $NO_2$ adsorption and reaction. The results could give insight into the structure–activity relationship of surface OH groups in OH-related surface reactions at a molecular level.

# Experimental section

### Preparation and characterization of $TiO_2$ samples

All samples were prepared from amorphous $TiO_2$ nanoparticles (206-11272, Wako Pure Chemical Industries, Ltd., with purity of 99.9% and average size of 50 nm) to eliminate the influence of commercial sources. Amorphous nano $TiO_2$ was used as purchased. Anatase and rutile $TiO_2$ samples were obtained by calcining amorphous $TiO_2$ at 873 and 1273 K for 3 h, respectively. The crystalline structure of the obtained samples was characterized using a powder X-ray diffractometer (XRD; X'Pert PRO, PANalytical, Netherlands) with Cu Kα ($\lambda$ = 0.154056 nm) radiation at 40 kV and 40 mA with scans from 10° to 90° in increments of 0.026°. The surface areas of the samples were measured with a physisorption analyzer (Autosorb-1C-TCD, Quantachrome, USA) by $N_2$ adsorption–desorption at 77 K. The surface area ($S_{BET}$) was determined by applying the Brunauer–Emmett–Teller (BET) method to the adsorption isotherm in the range of 0.05–0.35. The BET surface areas of the samples are summarized in Table S1 in the ESI.†

### *In situ* diffuse reflectance infrared Fourier transform spectroscopy (*in situ* DRIFTS) measurements

The heterogeneous reactions of $NO_2$ on $TiO_2$ samples were measured by *in situ* DRIFTS (Nicolet 6700, Thermo Fisher Scientific, USA), with an *in situ* diffuse reflection chamber and a high-sensitivity mercury cadmium telluride (MCT) detector cooled with liquid $N_2$. Before the experiment, $TiO_2$ samples were finely ground and placed into a ceramic crucible in the *in situ* chamber. The samples were first purged overnight in a stream of synthetic air (80% $N_2$ and 20% $O_2$) with a total flow of 100 mL $min^{-1}$. Then the samples were exposed to 200 ppmv $NO_2$ balanced with 100 mL $min^{-1}$ synthetic air for at least 3 h. All treatments and experiments were carried out at room temperature (303 K). The infrared spectra were collected using a computer with OMNIC 6.0 software (Nicolet Corporation, USA). All spectra were recorded at a resolution of 4 $cm^{-1}$ for 100 scans in the spectral range of 600 to 4000 $cm^{-1}$. The low frequency cutoff of the spectra was due to the strong lattice oxide absorption of the samples.

### Density functional theory (DFT) calculations

All calculations were performed using the Perdew–Burke–Ernzerhof (PBE) functional[24] as implemented in the Vienna *ab initio* simulation package (VASP).[25] The projector augmented wave method (PAW)[25,26] was used to describe the interaction between the ions and the electrons.[26,27] The energy cutoff of the plane wave was taken to be 400 eV. A (2 × 3) supercell of the anatase (101) surface with four stoichiometric $TiO_2$ layers was used (Fig. 1) and the vacuum gap was set at 20 Å. During geometrical optimization, the $NO_2$ molecule and the two top $TiO_2$ layers of the slab were allowed to relax, while the two bottom layers were fixed at their bulk position. Atoms were relaxed until forces were smaller than 0.05

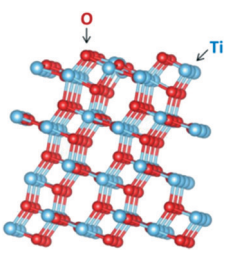


Fig. 1 Anatase (101) surface model used in the DFT calculation. Blue and red balls represent Ti and O atoms, respectively.

eV Å$^{-1}$. The Brillouin zone was sampled using a Monkhorst–Pack 2 × 2 × 1 mesh. The Gaussian smearing method with a smearing width of 0.2 eV was employed to accelerate the convergence of integration in the Brillouin zone.

The minimum energy paths (MEP) and transition states of the reactions were calculated using the climbing image nudged elastic band (CI-NEB) method, with a spring constant of 5.0 eV Å$^{-2}$ to restrain the images on the elastic band.[28] The initial structures of the intermediate images (six to nine images in the present calculations) were interpolated linearly from the optimized reactant (initial state) and product (final state) configurations. The vibrational frequencies were calculated using the finite difference approach with a step size of 0.015 Å.

## Results and discussion

### Reactions of $NO_2$ on $TiO_2$ samples

Reactions of $NO_2$ on $TiO_2$ with various crystal structures including amorphous, anatase, and rutile phases were investigated using *in situ* DRIFTS. Anatase and rutile $TiO_2$ were obtained by calcining amorphous $TiO_2$ at 873 and 1273 K for 3 h, respectively, as verified by the XRD patterns shown in Fig. 2.

The *in situ* DRIFTS spectra of the $TiO_2$ samples exposed to $NO_2$ for 3 h are shown in Fig. 3. The peaks observed in the range of 1200–1700 cm$^{-1}$ are due to the formation of surface species, while the negative peaks in the range of 3600–3800 cm$^{-1}$ were attributed to the consumption of surface OH groups. Detailed assignments of the surface species are summarized in Table S2.†

The main peaks in the range of 1200–1650 cm$^{-1}$, as the characteristic vibrations of nitrate species, implied that nitrates were the dominant surface products on $TiO_2$ regardless of the crystal structure. This is in accordance with the previous literature on the adsorption of $NO_2$ on $TiO_2$.[29–31] However, several distinctions exist among the reactions of $NO_2$ on amorphous, anatase, and rutile $TiO_2$. Firstly, the intensities of the nitrate peaks as well as the negative peaks of surface OH on rutile were much weaker than those on amorphous and anatase $TiO_2$, suggesting that rutile $TiO_2$ is less reactive toward $NO_2$. This might be due to its small specific surface area (4.6 m$^2$ g$^{-1}$), which provided a minimal amount of active sites. Secondly, nitrite, with a band at 1195 cm$^{-1}$, was observed at the beginning of the reaction and disappeared after the generation of nitrates on amorphous and anatase $TiO_2$ (Fig. S1†). This is in agreement with the previous finding that nitrite is a critical intermediate for the $NO_2$ reaction on Ti atoms.[18]

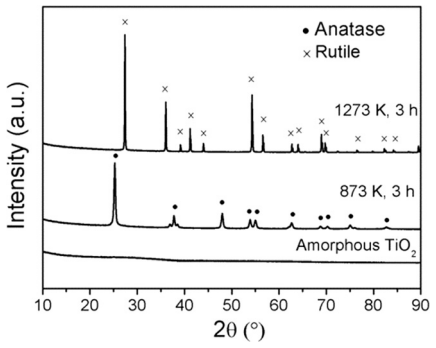


Fig. 2 XRD patterns of $TiO_2$ samples. Amorphous $TiO_2$ was used as purchased. Anatase and rutile $TiO_2$ samples were obtained by calcining amorphous $TiO_2$ at 873 and 1273 K for 3 h, respectively.

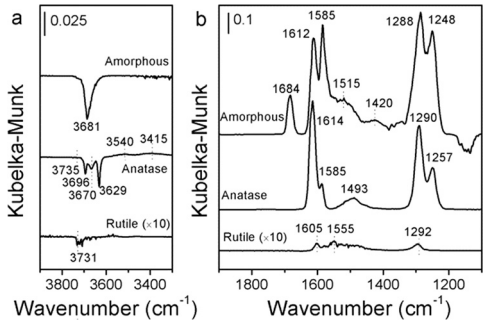


Fig. 3 *In situ* DRIFTS spectra of $NO_2$ reactions. (a) Consumption of OH groups after 3 h $NO_2$ reaction on amorphous, anatase, and rutile $TiO_2$. (b) Formation of surface species after 3 h $NO_2$ reaction on amorphous, anatase, and rutile $TiO_2$. Reaction conditions: 200 ppmv $NO_2$, 303 K, 3 h reaction, total flow of 100 mL min$^{-1}$ (80% $N_2$ and 20% $O_2$).

In addition, a band near 1684 cm$^{-1}$ was observed only on amorphous $TiO_2$. This band could be assigned to surface $HNO_3$ species rather than nitrate. For instance, two peaks at 1680 and 1310 cm$^{-1}$ were observed in the adsorption of $HNO_3$ on mineral oxides (such as $SiO_2$, $\alpha$-$Al_2O_3$, $TiO_2$, $\gamma$-$Fe_2O_3$, CaO, and MgO).[30,32–34] These two peaks were attributed to the asymmetric and symmetric stretching modes of surface-adsorbed $HNO_3$, respectively. In this work, the band at 1310 cm$^{-1}$ could be resolved by spectrum deconvolution fitting analysis (Fig. S2†). Moreover, a stable band at 1684 cm$^{-1}$ was observed in the adsorption of $HNO_3$ on amorphous and anatase $TiO_2$ (Fig. S3†), supporting the assignment of this peak to chemically adsorbed $HNO_3$ on the $TiO_2$ surface.

### Role of $H_2O$ and OH in $HNO_3$ formation

To our knowledge, this is the first time that the formation of surface-adsorbed $HNO_3$ has been detected during the $NO_2$ reaction on $TiO_2$ under dry and dark conditions. The generation of surface $HNO_3$ has been found in the reaction of $NO_2$ on UV-illuminated $TiO_2$ due to its combination with OH radicals.[21,35] Since the OH radicals were produced from the photolysis of surface water by UV-illumination, this reaction does not occur under dark conditions and could not contribute to the $HNO_3$ formation in this work.

Previous studies also showed that the disproportionation reaction between $NO_2$ and surface-adsorbed $H_2O$ leads to the formation of surface $HNO_3$ on the hydrated $SiO_2$ surface.[36–38] To determine the role of surface water in the formation of $HNO_3$ on amorphous $TiO_2$, the reactions of $NO_2$ on dehydrated and hydrated amorphous $TiO_2$ surfaces were compared (Fig. 4). For the hydrated amorphous $TiO_2$, the

 

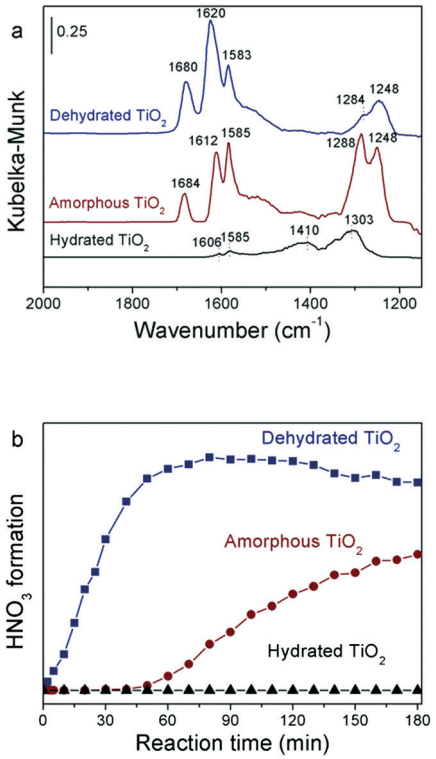


**Fig. 4** Effect of surface water on $HNO_3$ formation on amorphous $TiO_2$. (a) DRIFTS spectra obtained after 3 h $NO_2$ reaction on dehydrated amorphous $TiO_2$, hydrated amorphous $TiO_2$ and untreated amorphous $TiO_2$. (b) Comparison of $HNO_3$ formation during $NO_2$ reaction on dehydrated amorphous $TiO_2$, hydrated amorphous $TiO_2$ and untreated amorphous $TiO_2$. Dehydrated amorphous $TiO_2$ was obtained by heating at 423 K for 1 h, and then a dry $NO_2$ flow was introduced into the system. Hydrated $TiO_2$ was obtained by water absorption at 30% RH and 303 K for 1 h, and then a humid (30% RH) $NO_2$ flow was injected into the system. $NO_2$ reactions were carried out at 303 K for 3 h with a total flow of 100 mL $min^{-1}$ (80% $N_2$ and 20% $O_2$). The formation of $HNO_3$ was determined from the integrated areas of the $HNO_3$ bands at 1684 $cm^{-1}$ (for untreated amorphous $TiO_2$) and 1680 $cm^{-1}$ (for dehydrated amorphous $TiO_2$).

surface was first exposed to a humid air flow with a relative humidity (RH) of 30% for 1 h, and then 30% RH was maintained during the subsequent $NO_2$ reaction. Dehydrated amorphous $TiO_2$ was prepared by heating the samples at 423 K for 1 h before $NO_2$ reaction.

As shown in Fig. 4a, $NO_2$ reaction on hydrated amorphous $TiO_2$ leads to the formation of nitrates, in which water-solvated nitrate with bands at 1410 and 1303 $cm^{-1}$ is the dominant species.[18,36] The $HNO_3$ band at around 1680 $cm^{-1}$ was not detected on this hydrated surface. In contrast, it is clearly seen that $HNO_3$ (1680 $cm^{-1}$) formed on the dehydrated amorphous $TiO_2$ surface. Fig. 4b illustrates that $HNO_3$ formation on dehydrated $TiO_2$ was much faster than that on the untreated amorphous sample; meanwhile the amount of $HNO_3$ was greatly enhanced due to the desorption of surface water. These results verified the inhibiting effect of water adsorption on $HNO_3$ formation, implying that the disproportionation mechanism between $NO_2$ and $H_2O$ should not contribute to $HNO_3$ formation on amorphous $TiO_2$. In addition, adsorbed water could also lead to the dissociation of $HNO_3$ on the surface,[16] causing less molecularly adsorbed $HNO_3$ on hydrated $TiO_2$.

It should be noted that the formation of surface species was accompanied by the consumption of OH species, as shown in Fig. 3. These OH species should be important active sites for the $NO_2$ reaction. On amorphous $TiO_2$, only one OH group with a band at 3681 $cm^{-1}$ was consumed during the reaction. It is thus considered to be the active site for the formation of both $HNO_3$ and nitrate. Consumption of peaks at 3735, 3696, 3670, and 3629 $cm^{-1}$ was detected on anatase $TiO_2$, indicating that the reaction of $NO_2$ and OH species was more complicated on the anatase surface. On rutile $TiO_2$, the slight decrease in the intensity of the OH peak at 3731 $cm^{-1}$ together with the minimal generation of nitrates implied that the scarcity of active sites (*i.e.* OH groups) might contribute to the weak activity of the rutile surface. To further establish the role of OH species in the $NO_2$ reaction on $TiO_2$ samples, theoretical calculations were conducted to identify the structures of surface OH groups and explore the formation mechanism of surface products, especially surface-adsorbed $HNO_3$.

## Types of surface OH groups on $TiO_2$

Surface OH groups on metal oxides can be generally classified into isolated (or free) OH and hydrogen-bonded OH.[1,39,40] The difference between them is whether OH interacts with adjacent OH groups *via* hydrogen bonding. According to previous infrared studies, the absorption frequencies of isolated OH groups on $TiO_2$ surfaces are always higher than those of H-bonded OH groups.[1,40] For example, Primet *et al.* assigned high (3715 $cm^{-1}$) and low (3665 $cm^{-1}$) frequency bands detected on anatase to isolated and H-bonded OH groups, respectively.[40] Isolated OH groups could be further categorized into terminal and bridging OH groups on the $TiO_2$ surface.[1,39–41] The assignment of the infrared peaks of these isolated OH groups still remains controversial. Some infrared research based on the work of Primet *et al.*[40] and Tsyganenko *et al.*[1] proposed that the OH stretching frequency decreased from terminal OH (at around 3725 $cm^{-1}$) to bridging OH (at ~3670 $cm^{-1}$);[42,43] whereas Jackson and Parfitt[39] supposed that the thermally stable infrared peak at 3725 $cm^{-1}$ should be bridging OH, because it has a higher stability due to its bidentate attachment. Other authors also attributed the lower frequency at 3666 $cm^{-1}$ to terminal OH.[44]

DFT calculation, which is widely used for the study of surface chemistry on $TiO_2$,[45,46] was conducted in this work to establish the infrared frequency of various OH groups and explore their activity toward $NO_2$. Based on the previous studies, we supposed that terminal, bridging and H-bonded OH groups exist on $TiO_2$. The geometric structures of these OH groups are shown in Fig. 5. Anatase $TiO_2$, which possesses the most diverse hydroxyls, was chosen as the representative for the DFT study. A (2 × 3) supercell of the anatase

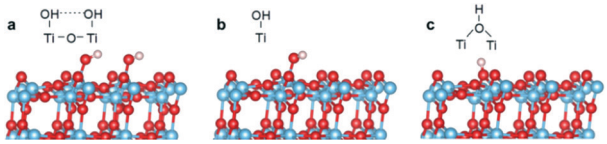


Fig. 5 Geometric structures of OH groups on anatase (101) surfaces. (a) H-bonded terminal OH groups. (b) Isolated terminal OH group. (c) Isolated bridging OH group. Blue, red, and pink balls represent Ti, O, and H atoms, respectively.

(101) surface plane with four stoichiometric layers (Fig. 1) was used in the calculations.

DFT-calculated vibrational frequencies are typically overestimated due to the harmonic approximation, and the anharmonic correction has been estimated to be about 72 $cm^{-1}$ for OH stretching frequencies, as estimated by Arrouvel *et al.*[47] Therefore, the calculated frequencies presented in Table 1 were obtained by subtracting the anharmonic correction. As listed in Table 1, the calculated frequencies of OH stretching modes increased from 3624 $cm^{-1}$ (H-bonded OH, with another band at 3659 $cm^{-1}$) to 3627 (terminal OH) and 3727 $cm^{-1}$ (bridging OH). According to this trend of frequency, the OH bands observed on anatase $TiO_2$ during the DRIFTS experiments were attributed to H-bonded (3629, 3696 $cm^{-1}$), terminal (3670 $cm^{-1}$), and bridging (3735 $cm^{-1}$) OH groups. The band at 3681 $cm^{-1}$ on amorphous $TiO_2$ was assigned to the terminal OH group, while the band at 3731 $cm^{-1}$ on rutile $TiO_2$ corresponded to the bridging OH group.

### Reactivity of OH groups toward $NO_2$

To investigate the reactivity of OH groups toward $NO_2$, the MEP of $NO_2$ reaction with H-bonded, terminal, and bridging OH groups on the anatase (101) surface was predicted by DFT calculations, as shown in Fig. 6.

When the $NO_2$ molecule approached one OH of the H-bonded hydroxyl (Fig. 6a), the $NO_2$ rotated around its N atom towards the O atom of the hydroxyl. Then the Ti–OH bond was weakened and formed a bond with the $NO_2$, forming an adsorbed $HNO_3$ species. The H atom of $HNO_3$ further transferred to the adjacent OH group, generating an adsorbed $H_2O$ molecule and a monodentate nitrate. This process is barrier-less and exothermic, indicating that the reaction of $NO_2$ with the H-bonded OH group is quite facile.

The reaction pathway of H-bonded OH and $NO_2$ on anatase could be verified by the DRIFTS experiment shown in Fig. S1b.† Quantitative analysis of H-bonded OH and monodentate nitrate on the anatase surface was conducted by integrating the areas of the relevant bands (Fig. 7). The results indicated that the consumption of H-bonded OH (3696 and 3629 $cm^{-1}$) accompanied the formation of monodentate nitrate (1493 $cm^{-1}$). The intensities of the two broad bands with centers at 3540 and 3415 $cm^{-1}$ increased as the reaction proceeded. These bands are attributed to the O–H stretching vibration of surface $H_2O$.[30,48] The H–O–H bending vibration of $H_2O$ at 1638 $cm^{-1}$ was also detected at the beginning of the reaction, which then overlapped with the strong vibration band of bridging nitrate at 1614 $cm^{-1}$.[30,48] These bands indicated the generation of surface-bound water during the reaction.

As shown by the MEP in Fig. 6b, the reaction of $NO_2$ with terminal OH resulted in the formation of adsorbed $HNO_3$. This reaction took place without any energy barrier, indicating that the terminal OH group is quite active in the $NO_2$ reaction. This reaction could explain the formation of surface-adsorbed $HNO_3$ during the $NO_2$ reaction on amorphous $TiO_2$. Although only the terminal OH group was consumed during the $NO_2$ reaction on amorphous $TiO_2$, various surface products, including both $HNO_3$ and nitrates, were generated (Fig. 3). The results suggest that $HNO_3$ is the final surface species in the reaction of terminal OH and $NO_2$ only if the OH group is isolated from other OH groups. Otherwise, $HNO_3$ will act as an intermediate and react with the adjacent OH groups, leading to the formation of nitrate species:

$$\begin{array}{ccccccc} HNO_3 & & OH & & NO_3 & & H_2O \\ | & + & | & \rightarrow & | & + & | \\ Ti & & Ti & & Ti & & Ti \end{array} \quad (1)$$

Due to its disordered structure, amorphous $TiO_2$ possesses plentiful defects such as oxygen vacancies and step

Table 1 Types of OH species on $TiO_2$ and their vibration frequencies

| OH species | Representation[a] | DFT calculation[b] ($cm^{-1}$) | DRIFTS measurement ($cm^{-1}$) |
|---|---|---|---|
| H-Bonded OH | OH ····· OH<br>\| \|<br>Ti—O—Ti | 3624, 3659 | 3629, 3696 (anatase) |
| Terminal OH | OH<br>\|<br>Ti | 3627 | 3670 (anatase)<br>3681 (amorphous) |
| Bridging OH | H<br>O<br>Ti Ti | 3727 | 3735 (anatase)<br>3731 (rutile) |

[a] Drawn according to the work of Tsyganenko *et al.*[1] [b] Anatase $TiO_2$ (101) surface with four stoichiometric $TiO_2$ layers was used in the DFT calculations.

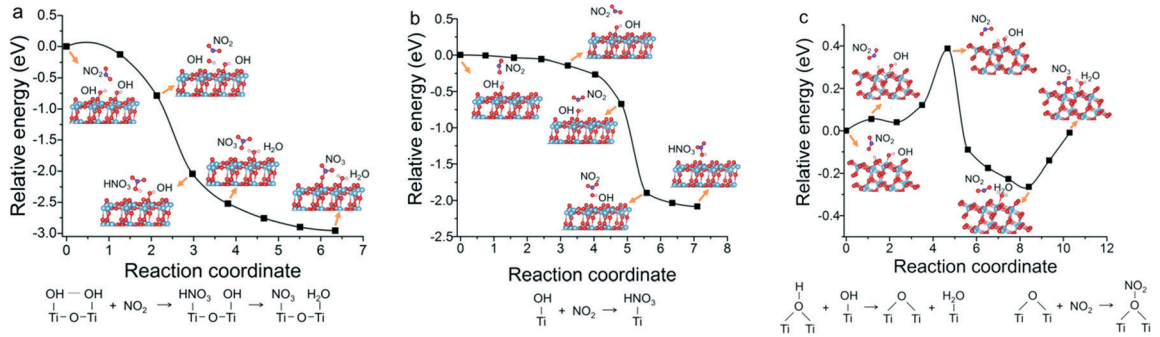


**Fig. 6** Minimum energy paths for $NO_2$ reactions on anatase $TiO_2$. (a) $NO_2$ reacting with the H-bonded OH group. (b) $NO_2$ reacting with the terminal OH group. (c) $NO_2$ reacting with bridging OH. The images show the initial and final configurations, as well as the representative intermediate images. Blue, red, pink, and purple balls represent Ti, O, H, and N atoms, respectively.

edges.[19,49,50] Thus, isolated OH groups instead of H-bonded OH groups might be dominant on amorphous $TiO_2$, and formation of $HNO_3$ was observable on this disordered surface.

As illustrated in Fig. 6c, bridging OH tended to react with the adjacent terminal OH groups. An adsorbed $H_2O$ molecule was the product of this process, and had the lowest energy in this MEP. This process was exothermic by 0.26 eV, with an energy barrier of 0.39 eV. In the lowest-energy configuration, the $NO_2$ molecule interacted with the deprotonated bridging oxygen and was stabilized by the electrostatic attraction between the positively charged N atom and the negatively charged surface O atom. When the $NO_2$ molecule moved closer to the deprotonated bridging oxygen, an adsorbed $NO_3^-$ species was formed. The increase in steric repulsion between the approaching $NO_2$ and the adjacent surface $H_2O$ gave rise to an increase in the energy of the adsorbed nitrate at the bridging site. Therefore, this process was endothermic by 0.25 eV. It is implied that the activity of bridging OH with $NO_2$ is quite weak, and nitrate formation *via* this reaction is unlikely. As illustrated by the DRIFTS experiment (Fig. 3), bridging OH was the dominant OH group consumed on the rutile surface. Therefore, besides the lack of active sites, the weak reactivity of rutile $TiO_2$ with $NO_2$ could be also attributed to the inactivity of bridging OH.

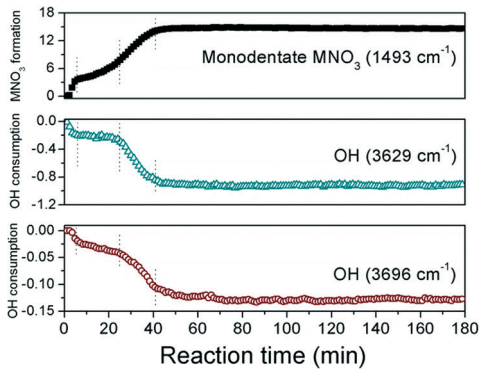


**Fig. 7** Comparison of nitrate formation and OH consumption on anatase $TiO_2$. Nitrate formation and OH consumption were represented by the integrated areas of the bands corresponding to monodentate nitrate (1493 $cm^{-1}$) and OH species (3629 and 3696 $cm^{-1}$). Reaction conditions: 200 ppmv $NO_2$, 303 K, total flow of 100 mL $min^{-1}$ (80% $N_2$ and 20% $O_2$).

## Conclusions

In this study, we observed an excellent example illustrating the structure–activity relationship of surface OH groups during $NO_2$ reaction on $TiO_2$ and the generation of special nitrogen-containing species. The results showed that the activities of H-bonded and terminal OH groups are much higher than that of bridging OH groups. Isolated terminal OH on amorphous $TiO_2$ dominates the reaction with $NO_2$, which resulted in the formation of chemisorbed $HNO_3$. Meanwhile, H-bonded OH on anatase exhibited a different reactivity toward $NO_2$, which gave rise to the formation of the intermediates $HNO_3$ and monodentate nitrate. In contrast, bridging OH, as the primary type of OH on the rutile surface, led to its weak reactivity toward $NO_2$. These results demonstrated that the reaction mechanism of $NO_2$ with $TiO_2$ is greatly dependent on the structure of OH groups.

Previous studies have shown that anatase is active in both catalysis and photocatalysis, and is the most used polymorph of $TiO_2$.[15,46,51,52] Although several factors such as facets and surface areas have been considered to contribute to the high activity of anatase,[53] the type and activity of surface OH groups might also play a critical role. The present work demonstrated that the crystal phase of $TiO_2$ determines the nature of the surface OH groups, which then determines the reaction of $NO_2$ on $TiO_2$. These results may also provide a potential formation pathway of nitrate *via* the $HNO_3$ intermediate on atmospheric nanoparticles having plenty of OH groups.

## Conflicts of interest

There are no conflicts to declare.

## Acknowledgements

This research was financially supported by the National Key R&D Program of China (2016YFC0202700) and the National Natural Science Foundation of China (41305116). The authors

also appreciate the Youth Innovation Promotion Association, CAS (2017064).

## Notes and references

1 A. A. Tsyganenko and V. N. Filimonov, *Spectrosc. Lett.*, 1972, **5**, 477–487.
2 J. C. Lavalley, *Catal. Today*, 1996, **27**, 377–401.
3 R. Atkinson, *Atmos. Environ.*, 2000, **34**, 2063–2101.
4 S. S. Brown, T. B. Ryerson, A. G. Wollny, C. A. Brock, R. Peltier, A. P. Sullivan, R. J. Weber, W. P. Dubé, M. Trainer, J. F. Meagher, F. C. Fehsenfeld and A. R. Ravishankara, *Science*, 2006, **311**, 67–70.
5 J. G. Calvert, A. Lazrus, G. L. Kok, B. G. Heikes, J. G. Walega, J. Lind and C. A. Cantrell, *Nature*, 1985, **317**, 27–35.
6 A. Indarto, *Res. Chem. Intermed.*, 2012, **38**, 1029–1041.
7 R. Rahila and M. Siddiqui, *Int. Res. J. Environ. Sci.*, 2014, **3**, 70–73.
8 J. C. Matsubu, V. N. Yang and P. Christopher, *J. Am. Chem. Soc.*, 2015, **137**, 3076–3084.
9 X. Chen, L. Liu, Y. Y. Peter and S. S. Mao, *Science*, 2011, **331**, 746–750.
10 F. Giordano, A. Abate, J. P. C. Baena, M. Saliba, T. Matsui, S. H. Im, S. M. Zakeeruddin, M. K. Nazeeruddin, A. Hagfeldt and M. Graetzel, *Nat. Commun.*, 2016, **7**, 10379.
11 J. Bai and B. Zhou, *Chem. Rev.*, 2014, **114**, 10131–10176.
12 P. Granger and V. I. Parvulescu, *Chem. Rev.*, 2011, **111**, 3155–3207.
13 X. Chen, P. Wang, P. Fang, H. Wang, C. Cen, W. Zeng and Z. Wu, *Environ. Sci.: Nano*, 2017, **4**, 437–447.
14 Q. Wu and R. van de Krol, *J. Am. Chem. Soc.*, 2012, **134**, 9369–9375.
15 H. Chen, C. E. Nanayakkara and V. H. Grassian, *Chem. Rev.*, 2012, **112**, 5919–5948.
16 M. Tang, D. J. Cziczo and V. H. Grassian, *Chem. Rev.*, 2016, **116**, 4205–4259.
17 J. A. Rodriguez, T. Jirsak, G. Liu, J. Hrbek, J. Dvorak and A. Maiti, *J. Am. Chem. Soc.*, 2001, **123**, 9597–9605.
18 G. M. Underwood, T. M. Miller and V. H. Grassian, *J. Phys. Chem. A*, 1999, **103**, 6184–6190.
19 U. Diebold, *Surf. Sci. Rep.*, 2003, **48**, 53–229.
20 K. Hadjiivanov, V. Bushev, M. Kantcheva and D. Klissurski, *Langmuir*, 1994, **10**, 464–471.
21 J. S. Dalton, P. A. Janes, N. G. Jones, J. A. Nicholson, K. R. Hallam and G. C. Allen, *Environ. Pollut.*, 2002, **120**, 415–422.
22 C. E. Nanayakkara, W. A. Larish and V. H. Grassian, *J. Phys. Chem. C*, 2014, **118**, 23011–23021.
23 M. M. Kantcheva, V. P. Bushev and K. I. Hadjiivanov, *J. Chem. Soc., Faraday Trans.*, 1992, **88**, 3087–3089.
24 J. P. Perdew, K. Burke and M. Ernzerhof, *Phys. Rev. Lett.*, 1996, **77**, 3865–3868.
25 G. Kresse and J. Furthmüller, *Phys. Rev. B: Condens. Matter Mater. Phys.*, 1996, **54**, 11169–11186.
26 P. E. Blöchl, *Phys. Rev. B: Condens. Matter Mater. Phys.*, 1994, **50**, 17953–17979.
27 G. Kresse and D. Joubert, *Phys. Rev. B: Condens. Matter Mater. Phys.*, 1999, **59**, 1758–1775.
28 G. Henkelman, B. P. Uberuaga and H. Jónsson, *J. Chem. Phys.*, 2000, **113**, 9901–9904.
29 C. Liu, Q. Ma, Y. Liu, J. Ma and H. He, *Phys. Chem. Chem. Phys.*, 2012, **14**, 1668–1676.
30 A. L. Goodman, E. T. Bernard and V. H. Grassian, *J. Phys. Chem. A*, 2001, **105**, 6443–6457.
31 Q. Ma, Y. Liu and H. He, *J. Phys. Chem. A*, 2008, **112**, 6630–6635.
32 A. M. Rivera-Figueroa, A. L. Sumner and B. J. Finlayson-Pitts, *Environ. Sci. Technol.*, 2003, **37**, 548–554.
33 J. Baltrusaitis, J. Schuttlefield, J. H. Jensen and V. H. Grassian, *Phys. Chem. Chem. Phys.*, 2007, **9**, 4970–4980.
34 Y. Fang, M. Tang and V. H. Grassian, *J. Phys. Chem. A*, 2016, **120**, 4016–4024.
35 Y. Bedjanian and A. El Zein, *J. Phys. Chem. A*, 2012, **116**, 1758–1764.
36 A. L. Goodman, G. M. Underwood and V. H. Grassian, *J. Phys. Chem. A*, 1999, **103**, 7217–7223.
37 B. J. Finlayson-Pitts, L. M. Wingen, A. L. Sumner, D. Syomin and K. A. Ramazan, *Phys. Chem. Chem. Phys.*, 2003, **5**, 223–242.
38 G. Lammel and J. N. Cape, *Chem. Soc. Rev.*, 1996, **25**, 361–369.
39 P. Jackson and G. D. Parfitt, *Trans. Faraday Soc.*, 1971, **67**, 2469–2483.
40 M. Primet, P. Pichat and M. V. Mathieu, *J. Phys. Chem.*, 1971, **75**, 1216–1220.
41 M. A. Henderson, *Langmuir*, 1996, **12**, 5093–5098.
42 H. Lin, J. Long, Q. Gu, W. Zhang, R. Ruan, Z. Li and X. Wang, *Phys. Chem. Chem. Phys.*, 2012, **14**, 9468–9474.
43 L. Ferretto and A. Glisenti, *Chem. Mater.*, 2003, **15**, 1181–1188.
44 Y. Lei, B. Liu, J. Lu, J. A. Libera, J. P. Greeley and J. W. Elam, *J. Phys. Chem. C*, 2014, **118**, 22611–22619.
45 M. Setvin, J. Hulva, H. Wang, T. Simschitz, M. Schmid, G. S. Parkinson, C. Di Valentin, A. Selloni and U. Diebold, *J. Phys. Chem. C*, 2017, **121**, 8914–8922.
46 A. Vittadini, M. Casarin and A. Selloni, *Theor. Chem. Acc.*, 2007, **117**, 663–671.
47 C. Arrouvel, M. Digne, M. Breysse, H. Toulhoat and P. Raybaud, *J. Catal.*, 2004, **222**, 152–166.
48 H. A. Al-Hosney and V. H. Grassian, *Phys. Chem. Chem. Phys.*, 2005, **7**, 1266–1276.
49 X. Zhou, V. Häublein, N. Liu, N. T. Nguyen, E. M. Zolnhofer, H. Tsuchiya, M. S. Killian, K. Meyer, L. Frey and P. Schmuki, *Angew. Chem., Int. Ed.*, 2016, **55**, 3763–3767.
50 M. A. Vargas and J. E. Rodríguez-Páez, *J. Non-Cryst. Solids*, 2017, **459**, 192–205.
51 K. I. Hadjiivanov and D. G. Klissurski, *Chem. Soc. Rev.*, 1996, **25**, 61–69.
52 N. Liu, C. Schneider, D. Freitag, U. Venkatesan, V. Marthala, M. Hartmann, B. Winter, E. Spiecker, A. Osvet and E. M. Zolnhofer, *Angew. Chem.*, 2014, **126**, 14425–14429.
53 W. Q. Fang, X. Q. Gong and H. G. Yang, *J. Phys. Chem. Lett.*, 2011, **2**, 725–734.

 